Microstructural studies of organic light-emitting devices by Monte Carlo simulation of two-dimensional triangles

Siew-Yen Cheng,[1] Jian-Sheng Wang,[2] and Gu Xu[1,3]
[1]*Department of Materials Science, National University of Singapore, Singapore 119260*
[2]*Department of Computational Science, National University of Singapore, Singapore 119260*
[3]*Department of Materials Science and Engineering, McMaster University, Hamilton, Canada L8S 4L7*
(Received 18 January 2000; revised manuscript received 12 June 2000)

The fast degradation of organic light-emitting devices (OLEDs) remains as the main obstacle to the commercialization of OLEDs. Among the failure mechanisms proposed, crystallization of the amorphous Alq_3 film that leads to the quenching of electroluminescence plays a crucial role and is little understood. Because *in situ* studies of the Alq_3 layer, with the probing of thin organic film by, for example, x-ray diffraction, are very difficult, if not impossible, Monte Carlo simulation is therefore conducted. The molecular motion of Alq_3 is simulated by two-dimensional triangles which interacted with a square-well potential in an isothermal-isobaric ensemble. Simulated results show the structural relaxation of Alq_3 from amorphous to crystalline upon thermal annealing. To impede this ordering process, quenched impurities of various shapes were added to the system. It is found that impurities of circular shape and of low aspect ratio have relatively the highest disordering effect. This is in good agreement with the experimental results. In addition, the preferred geometry of the Alq_3 system was also examined.

I. INTRODUCTION

Organic light-emitting devices (OLEDs) have been predicted by many as future flat panel displays for the information era, due to their low-voltage requirement, low cost, high quantum efficiency, and the wide color spectrum achievable.[1] These advantages have in recent years stimulated much research in this area. They include the development of OLEDs as display panels,[2–4] material studies,[5] the understanding of the charge transport and electroluminescence process,[6–8] and degradation studies.[9–14]

Although the lifetime of OLEDs has been dramatically improved thorough the years of studies as compared to when it was first introduced by Tang and Van Slyke in 1987,[16] the stability is still an issue. It becomes the major obstacle towards the commercialization of OLEDs. Possible mechanisms responsible for the degradation have been identified as morphological instability of the organic layers,[5,9–11] interdiffusion of the organic layers,[12] electrochemical reaction at the cathode/organic interface,[13] and recently the instability of the cationic Alq_3.[14] The latter, tris-(8-hydroxyquinoline) aluminum (III), has been widely used as the electroluminescence layer due to its high carrier transport property, amorphous film-forming ability,[12] and electrochemical stability.[15]

Crystallization of Alq_3 has been found to quench photons, but the reason behind such a process remains unclear despite possible explanations.[17,18] The interdiffusion process between Alq_3 and TPD (N,N'-diphenyl-N,N'-bis(3-methyl-phenyl)-(1,1′-biphenyl)-4,4′- diamine), a common hole transporting material in OLEDs,[12] has been debated as the main cause for the crystallization of Alq_3. But this interdiffusion process has been dissipated from reverse-current density studies of OLEDs[19] and from irreproducible results under a different atmospheric environment.[20] In addition, it was found that the crystallization process was induced by humidity.[17]

Other studies of Alq_3 crystallization were performed either on a thick, isolated layer of Alq_3[18] (relative to the thickness within the device) or on a device that involves the interplay of several degradation mechanisms occurring at the same time.[13,17] They lack convincing evidence as to whether such an ordering phenomenon really occurs in the device. The clarity of the above requires the structural analysis of the thin Alq_3 film buried within the multilayer device. *In situ* studies of the Alq_3 film, e.g., to probe thin organic film by x-ray diffraction, proved to be a formidable task.

Therefore, in this paper we try to study by Monte Carlo simulation the microstructural evolution of Alq_3 and the structural changes involved in the ordering process. The Alq_3 molecules were modeled by two-dimensional triangles to reflect the degradation mechanism via orientational ordering of Alq_3. This triangular model has not been explicitly included in the previous works on Monte Carlo simulation, which covered circular hard disks,[21–25] hard dumbbells,[26,27] cubes,[28] spherocylinders,[29] cut spheres,[30] ellipses,[31] Onsager crosses,[32] spheres,[33] and a mixture of different shapes.[34] Alder and Wainwright[35] were among the first to perform simulations on such hard body systems. To impede the orientational ordering of Alq_3, different shapes of impurities will be added to study their effect on the kinetics of this ordering process. Results will also be subsequently compared with the experimental data.

II. SIMULATION DETAILS

Throughout the simulation, a model of equilateral triangles was adopted to mimic the structure of Alq_3 (Ref. 36) in a two-dimensional system. The triangles are prohibited from overlapping by a hard core exclusion. The simulation was performed under periodic boundary conditions where

the triangles are accommodated in a unit cell of an infinite periodic lattice. Thus triangles that are displaced across the boundary to the neighboring cell would be equivalent to those being translated across to the opposite ends of the same cell. During the computation, in addition to the triangles within the same cell, the interactions with its periodic images have also to be taken into consideration.

Ergodicity is an important criterion in a valid Monte Carlo simulation[37] that requires the simulated results to be independent of the initial chosen state. At low temperatures, where displacement of the triangular molecules becomes smaller and slower, there would be a more prominent effect from the choice of initial configuration. Therefore, to minimize the influence of the choice of initial configuration, two different initial configurations are employed under an isothermal-isobaric ensemble (*NPT*). One of the initial configurations is ordered: the other is taken from the equilibrium random configuration at high temperature which is ''quenched'' to a new temperature by setting to the desired value.

Within this isothermal-isobaric ensemble, the parameters used are expressed in their reduced forms (dimensionless). For example, reduced pressure $P^*=P\sigma^2/\varepsilon$, reduced temperature $T^*=k_BT/\varepsilon$ and reduced volume (area to be exact) $V^*=V\sigma^2$, where σ is the unit length, ε is the potential height of the well, and k_B is Boltzmann's constant. A 12 $\times$12 unit cell was chosen, and the system consists of 200 triangles with the sides of each triangle taken to be unity, σ. A square-well potential was used to incorporate the temperature effect with the pair potential of the Alq_3 molecules defined Eq. (1),

$$V(r)=\begin{cases}\infty & \text{if two triangles overlap,}\\ -\varepsilon & \text{if } r<\sigma+\delta,\\ 0 & \text{if } r\geqslant\sigma+\delta,\end{cases} \tag{1}$$

where δ is the width of the square well potential [taken to be 1.4σ (Ref. 38)]. As described by the square-well potential, the interaction between a pair of triangles is repulsive when the triangles overlap and is attractive when outside the repulsive core. It should be noted that the orientation of the triangles was not taken into consideration during the potential evaluation.

The simulation was carried out for a temperature range of 0.05–5.0 under a fixed pressure of 10.0 or for a pressure range of 1.0–20.0 under a fixed temperature of 0.058. In the NPT ensemble, the simulation consists of two parts. One involves the displacement of the triangles; the other involves the change in the area of the cell. The displacement of a triangle is accepted if a random number generated uniformly in the interval of [0,1] is less than

$$\exp[-\beta(U'-U)], \tag{2}$$

where $\beta=1/(k_BT)$, and U and U' refer, respectively, to the energy before and after the displacement. In checking for overlapping, since it is local, the whole cell was divided into many smaller square boxes. The size of the boxes was chosen such that only the least number of triangles need to be checked for overlap in the neighboring eight boxes, in addition to the cell where the displaced triangle lies. This would save computing time even though it has to be updated each time, when the molecule is moved from one box to another. For the isotropic change in the area of the cell, it is accepted if the random number generated is less than

$$\exp\{-\beta[(U'-U)+P(V'-V)-(N+1)\beta^{-1}\ln(V'/V)]\}, \tag{3}$$

where N is the number of triangles.[39] The volume changes are time consuming and hence are computed with a probability of $1/N$ at each step. This change in the area (volume) involves the scaling of the coordinates of all the triangles. Both the area changes and triangle displacements follow the Metropolis scheme.[40]

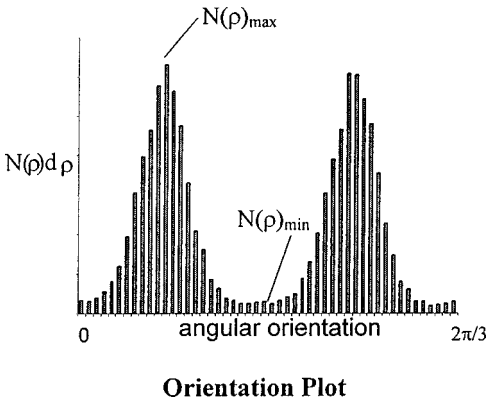

FIG. 1. Illustration of the definition of the orientation order parameter.

During the simulation, orientation plots are obtained to form histograms of the number of triangular molecules against their orientations. With the threefold symmetry associated with an equilateral triangle, only angles between 0 and $2\pi/3$ need to be investigated. From the orientation plot, an orientation order parameter φ is defined as follows and also illustrated in Fig. 1:

$$\varphi=\frac{N(\rho)_{\max}-N(\rho)_{\min}}{N(\rho)_{\max}+N(\rho)_{\min}}, \tag{4}$$

where $N(\rho)_{\max}$ and $N(\rho)_{\min}$ refer, respectively, to the maximum and minimum number of triangles within a certain angular interval. The orientation order parameter not only serves as a guide to the equilibration of the system, but also measures the degree of order (or disorder) of the system. Thus an orientation plot with uniform angular distribution will have a low orientation order parameter, while a plot that displays orientation preference will have a high orientation order parameter. The former points to a random system, and the latter indicates an ordered system.

III. RESULTS AND DISCUSSION

A. Glassy to orientational order transition of Alq_3

A system consisting of 200 triangles with a square-well potential was used in all simulations. The simulation was first performed with a constant pressure of 10.0 over a temperature range of 0.05–2.0 under the periodic boundary condition. Results were extracted after 10^6 Monte Carlo steps and shown by the plot of the orientation order parameter versus temperature (Fig. 2). The orientation order parameter describes the degree of ordering of the system, where a high

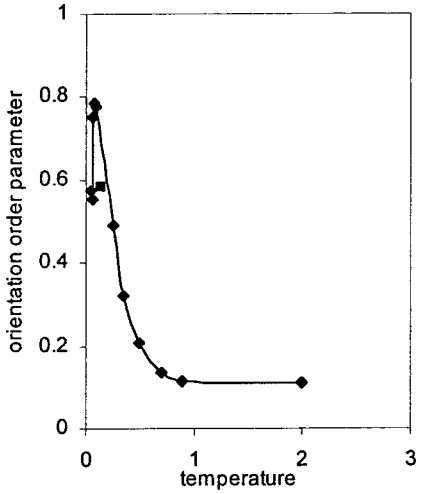

FIG. 2. Plot of the orientation order parameter vs reduced temperature obtained under the periodic boundary condition. The simulation was carried out with $N=200$, $P^*=10$, $\sigma^*=1$, and Monte Carlo steps of $1.48\times10^6-2.4\times10^6$.

orientation order parameter indicates a highly ordered system. This orientation order parameter is inversely correlated to the thermodynamic parameter of entropy. Therefore, a high orientation order parameter that indicates an ordered system is equivalent to the one of low entropy. Thus Fig. 2 reflects the change in the entropy of the system with temperature.

From Fig. 2, at $T^*\sim0.1$, the orientation order parameter was found to drop sharply as temperature increases, which corresponds to the transition from an orientation ordering to a random state. The orientation order parameter below $T^*\sim0.1$ again falls as the temperature decreases. This reflects the fact that the system becomes more disordered as temperature falls.

Three different states can thus be identified. Figures 3(a)–3(c) illustrate the configuration of the systems approaching equilibrium at (a) $T^*=0.05$, (b) $T^*=0.1$, and (c) $T^*=2.0$. They correspond to the amorphous, long-range orientation order, and random states as shown by their orientation plots. The presence of angular preference indicates a certain degree of ordering within the system, as seen in the orientation plots of Figs. 3(a) and 3(b). The uniform or random angular distribution of the orientation plot in Fig. 3(c) reflects a random state.

The drop in the orientation order parameter at temperatures below 0.1 indicates the formation of an amorphous phase. This is supported by the results in Fig. 3(a) where a glassy configuration of the system is observed. At temperatures higher than 0.1, the system has enough thermal energy to fluctuate and equilibrate into an ordered state of lowest energy. But at lower temperatures, the system lacks the thermal fluctuations needed to settle into the ordered state. Thus the system was caught in a metastable or nonequilibrium state, with frozen molecules. However, it was pointed out[41] that the sudden removal of kinetic energy generally produces a noncrystalline atomic configuration. This corresponds to the minimum potential energy reached by the steepest descent from the initial configuration. Such a process may not necessarily represent a glass transition despite a glassy configuration.

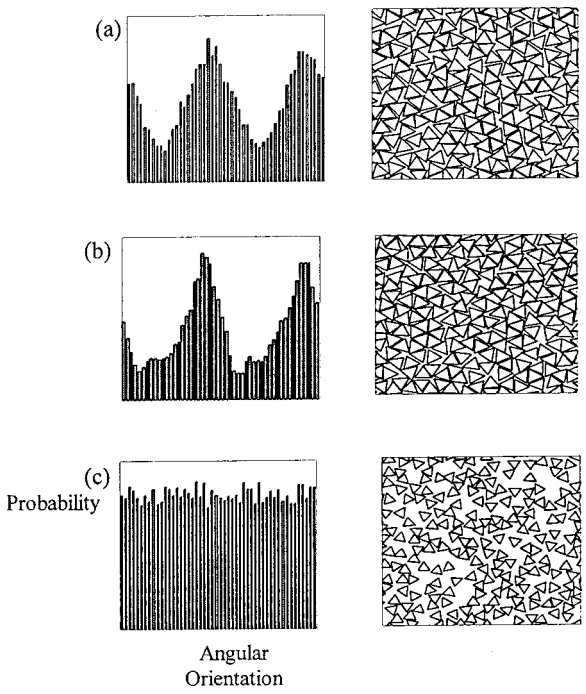

FIG. 3. (a)–(c) The figures illustrate the distinctive features of the various states obtained under the periodic boundary condition. Orientation plots (histograms of number of triangles against their orientations) are placed alongside the configurations of the systems. Comparing the different states, the orientation order of the different states is evident. (c) shows the random orientation of the system at $T^*=2.0$, (b) the angular preference of the orientation ordered phase at $T^*=0.1$, and (a) the glassy phase with slight orientation ordering at $T^*=0.05$. Triangles that intersect the boundary are translated across the opposite ends (periodic boundary effect).

Moreover, the glassy transition is also observed by a changing pressure under the isothermal condition, where the simulation was carried out over a pressure range of 1.0–20.0 at $T^*=0.058$. The temperature was chosen to be near the transition, as shown in Fig. 2, to shorten the computing time. Results were extracted after typical Monte Carlo steps of 10^6 and shown by the plot of orientation order parameter versus pressure (Fig. 4). From the plot, a peak at $P^*\sim5.0$ is

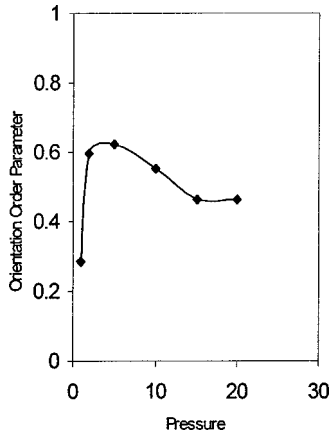

FIG. 4. Plot of the orientation order parameter vs reduced pressure obtained under the periodic boundary condition. The simulation was carried out with $N=200$, $T^*=0.058$, $\sigma^*=1$, and typical Monte Carlo steps of 10^6.

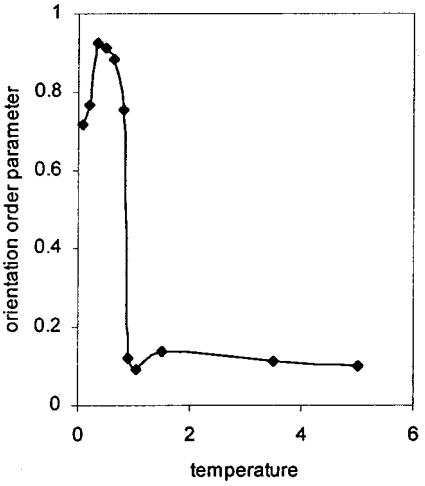

FIG. 5. Plot of the orientation order parameter vs reduced temperature obtained under hard wall boundary conditions. The simulation was carried out with $N=200$, $P^*=10$, $\sigma^*=1$, and Monte Carlo steps ranging from 400 000 to 900 000.

evident, where the orientation order parameter first increases and then falls as pressure increases. This result confirms the transitions found in Fig. 2. Both demonstrate similar orientation ordering to a glassy transition as the temperature decreases or as the pressure increases.

Under the constant pressure and temperature condition (*NPT*), the system is free (given enough time) to transform completely into the state of lowest free energy. While under the constant volume and temperature condition (*NVT*), the system may be prevented from phase separating into different densities due to its finite size.[39] Therefore, the structural studies were done under the NPT instead of the NVT condition. Moreover, the NPT condition is more realistic and closer to the real environment in a device.

The possible impact of the periodic boundary on the ordering phenomenon was investigated by changing the shape of the unit cell from a square to a rectangle with different aspect ratios. In addition, the size of the system was also changed to check for the size dependence. Similar plots to Fig. 2 were obtained. This means that the ordered phase is not constrained by the shape or size of the periodic cell.

To further study the effect of boundary in our system, simulation was also performed under the hard wall boundary. Figure 5 shows the plot of the orientation order parameter versus temperature, obtained with typical Monte Carlo Steps of 10^5. Similar transitions were also obtained. However, there is a quantitative difference in the temperature. This is due to the hard wall boundary that acted as impenetrable walls. As a result, the symmetry of the system was broken, which will ease the nucleation of crystal growth.[24] This also explains the longer equilibration time required for the periodic boundary. The quantitative difference may also be due to the effect of the small size of 200 triangles used in the system.

Although the simulation studies reveal the structural relaxation of Alq_3 from the amorphous to crystalline state, it should be pointed out that the results were obtained under thermodynamic equilibrium, and the kinetic requirement is not reflected. However, long-term usage of OLEDs requires extensive application of an electric current. With 90% of the power consumption converted into joule heat, this leads to the slow thermal annealing of amorphous organic layers. From our simulated results, this induces the structural relaxation of the Alq_3 layer. These were supported by experimental observation of the formation of crystallites from the Alq_3 layer.[9,18]

Such structural changes have a significant effect on the performance of OLEDs. Thickness variation of the thin Alq_3 film due to crystallization will lead to a local electric field concentration that may cause the growth of hot spots. These local hot spots will in turn promote the growth of crystals that are known to quench photons. In addition, dome formations from crystalline clusters may lead to the delamination of the Alq_3 layer from the electrode, which results in device failure.[17] It was also found that as the percentage of crystallinity increases, it leads to an increase in voltage under constant current and a drop in quantum efficiency.[42]

In the various works for the phase transitions of shaped particles, such as cubes,[28] spherocylinders,[29] cut spheres,[30] and ellipses,[31] there are many uncertainties on the existence of the cubatic[30,32] and hexatic[25] phases. The cubatic phase is a long-range orientationally ordered phase without any positional order of the particles, while the hexatic phase is an intermediate phase found before the transition from an ordered to an isotropic phase. The presence of such phases in our system would require further calculations and work, which is beyond our purpose here.

B. Microstructural evolution of Alq_3

To study the microstructure of the preferred geometry, we first introduce an orientation radial correlation function φ', which is defined as

$$\varphi' = \frac{\Sigma_{i=0}^{N-1}\Sigma_{j<i}^{n(r_{ij})}\cos(\phi_i-\phi_j)}{\Sigma_{i=0}^{N-1}\Sigma_{j<i}^{n(r_{ii})}n(r_{ij})}, \tag{5}$$

where the numerator is the summation of the cosine of the angular difference between each triangular pair and the denominator is the total number of triangular pairs with center-to-center separation of r_{ij}. As an example, the orientation radial correlation function at $T^*=0.5$ (Fig. 5) was plotted against the radial separation between the triangles, as shown in Fig. 6. When compared with Figs. 3(a) and 3(b), it is evident that the triangles tend to pack with two peak orientations differing by $\pi/3$. The inserted triangular pairs further illustrate the preferred packing geometry, where the radial separation and orientation difference match the peaks in Fig. 6.

This preferred packing geometry of the triangles is due to the fact that, when pointing in between the three vertices, the square-well potential has an attraction range extending beyond each side of a triangle. The sides of the triangle will thus have a wider region of attractive interactions as compare to the vertices of the triangle. This can be illustrated by the inserted triangle at the right bottom of Fig. 6. The circular boundary surrounding the triangle represents the radial distance of the attractive potential. Therefore, the wider attractive regions next to the sides of the triangles lead to the preference packing along their sides.

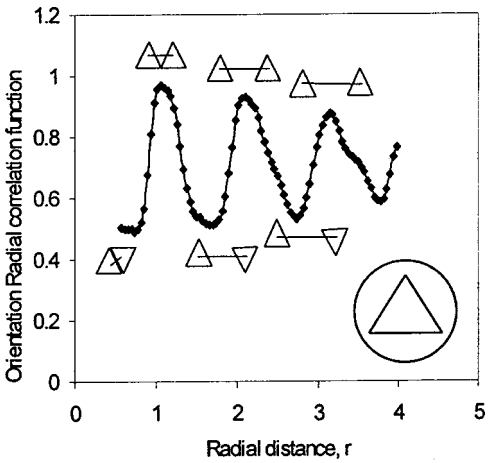

FIG. 6. Graph of the orientation radial correlation function vs radial distance for the system at $T^*=0.5$, $P^*=10$, $\sigma^*=1$, and $N=200$ after 480 000 Monte Carlo steps. The inserted triangular pairs illustrate the orientation difference between the triangular pairs as a function of distance. The circular boundary surrounding the triangle at the right bottom represents the radial distance of the attractive potential.

In reality, a two-dimensional equilateral triangle represents a two-dimensional projection of the three-dimensional Alq_3 molecule. Though this projection of the Alq_3 molecule is not always an equilateral triangle,[36] the approximation simplifies the computation and serves as a good starting point. Despite its simplicity, the model is able to describe the microscopic features of the system.

C. Effect of addition of different shaped impurities

Since the structural change of Alq_3 affects the lifetime of OLEDs, we try next to impede this ordering process through the addition of quenched impurities. The impurity effect was studied under the NPT condition at $T^*=0.5$ where the stable ordered phase was found in Fig. 5. The starting configurations of the system were formed by placing the impurities at random positions and orientations before the addition of triangles at random. Except for the exclusion between the triangles and impurities, the simulation was performed in the same way as that without impurities. The impurities are not moved except when the volume rescales.[39]

Table I lists the orientation order parameters affected by the added impurities of various shapes at equilibrium state. From the table, it can be found that the addition of impurities impedes, in general, the ordering process, because the systems containing the quenched impurities have much lower order parameters. Furthermore, two different trends can be observed from the table. First, as the aspect ratio of the impurities increases, the orientation order parameter increases. This indicates that impurities with higher aspect ratio have lower impedance. Second, for impurities of similar aspect ratio, circular impurities have a much higher impedance effect on the system than the square ones. This can be illustrated clearly from Figs. 7(a) and 7(b). Figure 7(a) shows that circular impurities are able to introduce disordering from all directions and thus able to impede the packing of the triangles. For the square impurities, they are able to align with the sides of the triangles [Fig. 7(b)]. Thus they enable more efficient packing and hence higher ordering. Therefore, the shape of the impurities plays a crucial role in the ordering process of the triangular system.

TABLE I. The orientation order parameters of the different doped systems reached at equilibrium are shown. The results are the average of three different random starting configurations of the quenched impurities. Impurities of 5% (number ratio) were studied under $T^*=0.5$, where stable order phase was found in the pure system. The area of each of the dopant used is approximately 30% of that of a triangle.

Impurity type	Aspect ratio	Orientation order parameter
(Pure)	0	0.9277
Circle	1	0.745
Square	1	0.8109
Rectangle	2	0.8128
Elongated Rectangle	3.911	0.8655

This result is significant as it can be used as an additional criterion for the choice of the dye dopant. OLEDs with

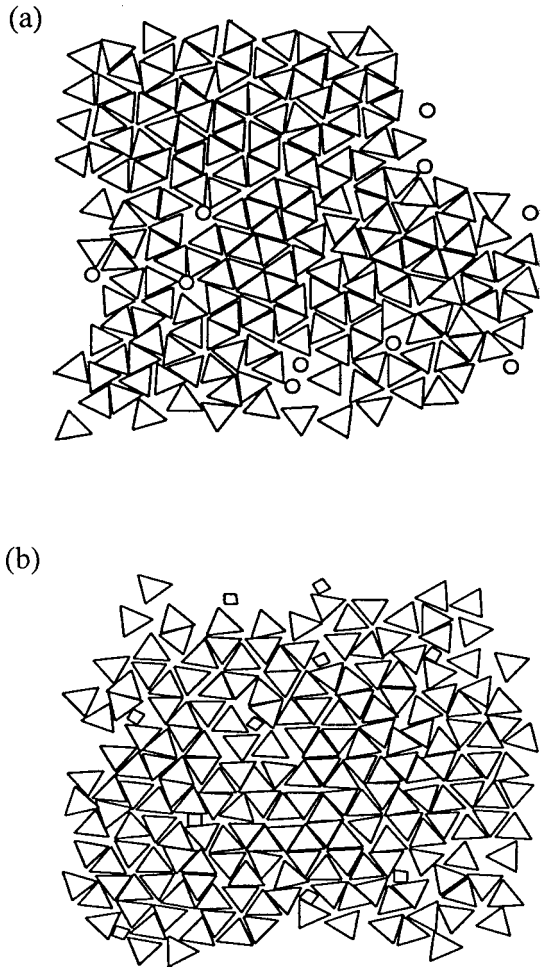

FIG. 7. Illustration of the greater impedance effect of circular impurities (a) as compared to the square impurities (b). Note the alignment of the square impurities with the sides of the triangles in (b).

TABLE II. The relative stabilities are extracted from the experimental results by Sato *et al.* (Ref. 15). Aspect ratios are estimated based on the rough bond lengths of the two-dimensional dopants. A relative stability of 1 refers to the dopant with the highest stabilization effect on OLEDs while 5 refers to the least stabilized doped system.

Relative stability	Dopants	Aspect ratio
1	Rubrene	Analogus to Circle
2	Perylene	1.155
2	9,10-diphenylanthracene	1.58
3	Decacyclene	Analogus to Triangular
4	Quinacridone	~4.33
5	undoped	

doped Alq_3 have been extensively used for increased stability and for the control of color emission.[15,43,44] When compared with the experimental results, it is interesting to see that our simulated results follow the same trends.[15] Table II lists the relative stability for the different doped systems by Sato *et al.*[15] The aspect ratios in Table II were estimated using rough bond lengths[45] with their molecular structures shown in Fig. 8.

From Table II and Fig. 8, it was found that rubrene has the highest stabilization effect on the lifetime of the OLEDs. Furthermore, as the aspect ratio increases, the stabilization effect of the dopants falls. This is in good agreement with our simulated results. It must also be emphasized that the above comparisons are based solely on the shape of the impurities. In addition, both rubrene and quinacridone are of comparable size; they are, however, far apart in terms of their stabilization effects. Thus it seems the size of the dopants does not play a significant role here. Of course, other factors such as the chemical structure and bonding[43] should also be accounted for the stability.

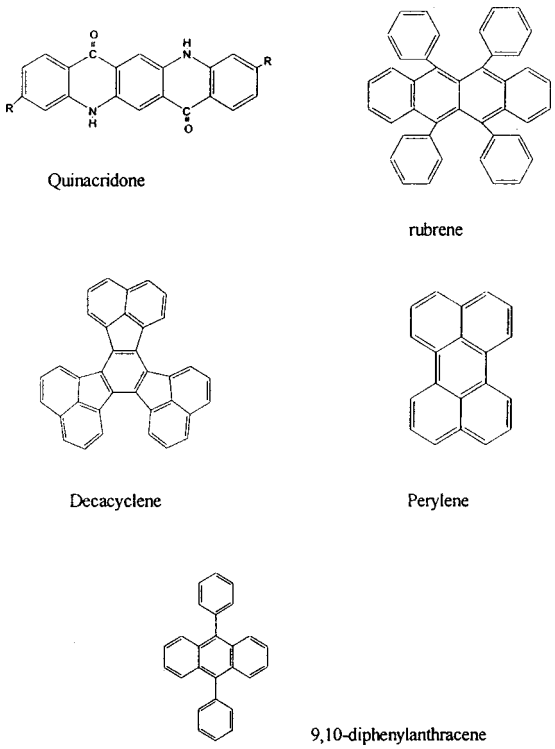

FIG. 8. Illustration of the molecular shapes of the dopants used by Sato *et al.* (Ref. 15) in their experimental works.

IV. CONCLUSIONS

From the above results, it is clear that the crystallization of Alq_3 plays an important role in the degradation of OLEDs. This is demonstrated by the Monte Carlo simulation of the dynamic structural relaxation of Alq_3. Impurities of circular shape and low aspect ratio seem to have the best impedance to the ordering process.

Even though the model adopted to simulate the Alq_3 molecules is rather simple, it allows for isolation from the interplay of other mechanisms involved in a multilayer device. The simulated results from this model have proved to be in good agreement with the experimental observations. In addition, it also confirms that triangular Alq_3 tends to pack with angular difference of $\pi/3$.

ACKNOWLEDGEMENT

The authors wish to express their thanks to Professor L. V. Woodcock for a helpful discussion and comments.

[1] J. R. Sheats, Homer Antoniadis, M. Hueschen, W. Leonard, J. Miller, R. Moon, D. Roitman, and A. Stoking, Science **273**, 884 (1996).
[2] G. Gu and S. R. Forrest, IEEE J. Sel. Top. Quantum Electron. **4**, 83 (1998).
[3] Y. Kijima, N. Asai, N. Kishii, and S-I. Tamura, IEEE Trans. Electron Devices **44**, 1222 (1997).
[4] P. E. Burrows, G. Gu, V. Bulović, Z. Shen, S. R. Forrest, and M. E. Thompson, IEEE Trans. Electron Devices **44**, 1188 (1997).
[5] C. Adachi, K. Nagai, and N. Tamoto, Appl. Phys. Lett. **66**, 2679 (1995).
[6] D. V. Khramtchenkov, H. Bässler, and V. I. Arkhipov, J. Appl. Phys. **79**, 9283 (1996).
[7] P. E. Burrows and S. R. Forrest, Appl. Phys. Lett. **64**, 2285 (1994).
[8] P. E. Burrows, Z. Shen, V. Bulović, D. M. McCarty, S. R. Forrest, J. A. Cronin, and M. E. Thompson, J. Appl. Phys. **79**, 7991 (1996).
[9] F. Papadimtrakopoulus, X-M. Zhang, and K. A. Higginson, IEEE J. Sel. Top. Quantum Electron. **4**, 49 (1998).
[10] H. Tanaka, S. Tokito, Y. Taga, and A. Okada, Chem. Commun. (Cambridge) **18**, 2175 (1996).
[11] E. M. Ham, L-M. Do, Y. Niidome, and M. Fujihira, Chem. Lett. **57**, 969 (1994).
[12] E. M. Ham, L. M. Do, N. Yamamoto, and M. Fujihira, Thin Solid Films **273**, 202 (1996).

[13] H. Aziz, Z. Popovic, C. P. Tripp, N. X. Hu, A. M. Hor, and G. Xu, Appl. Phys. Lett. **72**, 2645 (1998).
[14] H. Aziz, Z. D. Popovic, N-X. Hu, Ah-Mee Hor, and G. Xu, Science **283**, 1900 (1999).
[15] Y. Sato, S. Ichinosawa, and H. Kanai, IEEE J. Sel. Top. Quantum Electron. **4**, 40 (1998).
[16] C. W. Tang and S. A. Van Slyke, Appl. Phys. Lett. **51**, 913 (1987).
[17] H. Aziz, Z. Popvic, S. Xie, Ah-Mee Hor, N. X. Hu, C. Tripp, and G. Xu, Appl. Phys. Lett. **72**, 756 (1998).
[18] K. A. Hugginson, X. M. Zhang, and F. Papadimitrakopulus, Thin Solid Films **10**, 1017 (1998).
[19] T. P. Nguyen, P. Jolinat, P. Destruel, R. Clrgereaux, and J. Farenc, Thin Solid Films **325**, 175 (1998).
[20] J. McElvain, H. Antoniadis, M. R. Hueschen, J. N. Miller, D. M. Roitman, and R. L. Moon, J. Appl. Phys. **80**, 6002 (1996).
[21] J. F. Fernández, J. J. Alonso, and J. Stankiewicz, Phys. Rev. Lett. **75**, 3477 (1995).
[22] F. F. Abraham, Phys. Rev. Lett. **44**, 463 (1980).
[23] J. Lee and K. Strandburg, Phys. Rev. B **46**, 11 190 (1992).
[24] J. F. Fernández, J. J. Alonso, and J. Stankiewicz, Phys. Rev. E **55**, 750 (1997).
[25] A. Jaster, Phys. Rev. E **59**, 2594 (1999).
[26] S. J. Singer and R. Mumaugh, J. Chem. Phys. **93**, 1278 (1990).
[27] C. Vegen, E. P. A. Paras, and P. A. Monson, J. Chem. Phys. **97**, 8543 (1992).
[28] M. Dijkstra and D. Frenkel, Phys. Rev. Lett. **72**, 298 (1994).
[29] R. V. Roij, P. Bolhuis, B. Mulder, and D. Frenkel, Phys. Rev. E **52**, R1277 (1995).
[30] R. Blaak, D. Frenkel, and B. Mulder, J. Chem. Phys. **110**, 11 652 (1999).
[31] J. A. Cuesta and D. Frenkel, Phys. Rev. A **42**, 2126 (1990).
[32] R. Blaak and B. M. Mulder, Phys. Rev. E **58**, 5873 (1998).
[33] L. Lue and L. V. Woodcock, Mol. Phys. **96**, 1435 (1999).
[34] P. A. Monson and M. Rigby, Mol. Phys. **39**, 989 (1980).
[35] B. J. Alder and T. E. Wainwright, J. Chem. Phys. **27**, 1207 (1957).
[36] M. Ul. Haque, W. Horne, and S. J. Iyle, J. Crystallogr. Spectrosc. Res. **21**, 411 (1991).
[37] W. W. Wood, in *Physics of Simple Liquids*, edited by H. N. V. Temperley, J. S. Rowlinson, and G. S. Rushbrooke (North-Holland, Amsterdam, 1968), Chap. 5.
[38] Y. Rosenfeld and R. Thieberger, J. Chem. Phys. **63**, 1875 (1975).
[39] D. Frenkel and B. Smith, *Understanding Molecular Simulation: From Algorithms to Applications* (Academic, San Diego, 1996), Chaps. 3 and 5.
[40] N. Metropolis, A. W. Rosenbluth, M. N. Rosenbluth, A. N. Teller, and E. Teller, J. Chem. Phys. **21**, 1087 (1953).
[41] J. Jäckle, Rep. Prog. Phys. **49**, 171 (1986).
[42] M. D. Joswick, I. H. Campbell, N. N. Barashkov, and J. P. Ferraris, J. Appl. Phys. **80**, 2883 (1996).
[43] J. Shi and C. W. Tang, Appl. Phys. Lett. **70**, 1665 (1997).
[44] T. Mori and T. Mizutani, Polym. Adv. Technol. **8**, 471 (1996).
[45] J. McMurry, *Organic Chemistry* (Pacific Grove, California, 1996).